Journal of Thermal Science Vol.30, No.4 (2021) 1251−1267

https://doi.org/10.1007/s11630-021-1475-7 **Article ID: 1003-2169(2021)04-1251-17**

Novel Matching Strategy for the Coupling of Heat Flux in Furnace Side and CO_2 Temperature in Tube Side to Control the Cooling Wall Temperatures

LIU Chao[1], MIAO Zheng[1,2*], XU Jinliang[1,2], XU Zeyu[1], LI Mingjia[3]

1. Beijing Key Laboratory of Multiphase Flow and Heat Transfer for Low Grade Energy Utilization, North China Electric Power University, Beijing 102206, China
2. Key Laboratory of Power Station Energy Transfer Conversion and System, North China Electric Power University, Ministry of Education, Beijing 102206, China
3. Key Laboratory of Thermo-Fluid Science and Engineering of Ministry of Education, School of Energy & Power Engineering, Xi'an Jiaotong University, Xi'an 710049, China

Abstract: Required by the supercritical carbon dioxide (sCO_2) coal-fired power cycle, sCO_2 entering a boiler has a high temperature and can cause overheating of tubes. To eliminate the pressure drop penalty effect, the sCO_2 boiler consists of several modules, each having different heat flux received from the furnace side (q) and different CO_2 temperature in the cooling wall tube (T_f). We aim to search for the best matching strategy coupling furnace side and tube side to obtain the lowest temperature of tubes. By theoretically analyzing the wall temperature influenced by q, T_f and a comprehensive thermal resistance C, two matching methods are introduced: the heat flux-temperature matching (HTM) which matches higher q with lower T_f, and the heat flux-heat flux matching (HHM) that matches higher q with higher allowable-heat-flux at the temperature limit of tubes. HTM is a conventional method but HHM is newly proposed here. We show that, if C is identical for different modules, the two methods coincide; otherwise, HHM is recommended. For a sCO_2 boiler driving 1000 MWe power plant, smaller cooling wall temperatures are obtained by HHM than HTM. Based on HHM, the mid-partition wall, heat transfer enhancement, and downward flow are comprehensively used, decreasing the wall temperature significantly.

Keywords: sCO_2 power cycle, sCO_2 modular boiler, cooling wall temperature, allowable heat flux, matching strategy

1. Introduction

At present, power generation throughout the world mainly relies on the water-steam power plants driven by fossil energy and other energies. Global warming and energy security motivate researchers to explore more efficient energy conversion solutions. Supercritical carbon dioxide (sCO_2) Brayton cycle is regarded as a game-changing technology to make a significant breakthrough. Compared with the supercritical water-steam cycle, the sCO_2 cycle can offer the following benefits: (1) higher cycle efficiency can be achieved

Received: Dec 16, 2020 AE: GOVARDHAN M. Corresponding author: MIAO Zheng E-mail: miaozheng@ncepu.edu.cn

Nomenclature

A	cross-sectional area per tube/m^2
C	comprehensive thermal resistance/$m^2 \cdot K \cdot kW^{-1}$
c	additional thickness/mm
d	diameter/mm
f	friction coefficient
h	enthalpy/$kJ \cdot kg^{-1}$
L	height of furnace/m
l	length of tube/m
M	total mass flow rate in a module/$kg \cdot s^{-1}$
m	mass flow rate per tube/$kg \cdot s^{-1}$
n	number of tubes in a heat exchanger module
P	pressure/MPa
P_f	friction pressure drop/MPa
Pr	Prandtl number
q	heat flux/$kW \cdot m^{-2}$
Q	thermal power/MWth
r	radial coordinate of the cylindrical coordinate, m
R	thermal resistance/$m^2 \cdot K \cdot kW^{-1}$
Re	Reynolds number
s	tube pitch, mm
T	temperature/°C
u	velocity/$m \cdot s^{-1}$
w	width or depth of furnace/m
z	coordinate along furnace height/m

Greek symbols

α	heat transfer coefficient/$W \cdot m^{-2} \cdot K^{-1}$
β	ratio of outer diameter to inner diameter
δ	thickness/mm
Δ	difference between allowable heat flux and local heat flux/$kW \cdot m^{-2}$; temperature difference/°C
φ	angle coefficient
φ_{min}	minimum reduction factor
η_q	non-uniformity coefficient of heat flux
ρ	density/$kg \cdot m^{-3}$
λ	thermal conductivity/$W \cdot (m \cdot K)^{-1}$
θ	circumferential coordinate of the cylindrical coordinate/rad
$[\sigma]$	allowable stress of the tube wall under allowable temperature
μ	heat distribution coefficient of the outer wall

Subscripts

ave	average
cd	heat conduction
cv	heat convection
e	enhanced heat transfer
f	fluid or fin
fin	fin tip
i	inner or the ith module
max	maximum
l	allowable
o	outer
out	outlet of tube
w	tube wall

Abbreviations

AP	air preheater
C	compressor
EAP	external air preheater
HHM	heat flux-heat flux matching
HTR	high temperature recuperator
LTR	low temperature recuperator
RH	reheater
SH	superheater in upper furnace
T	turbine
HTM	heat flux-temperature matching

when the main vapor temperature is higher than 550°C [1]; (2) the compactness of the sCO_2 cycle system enables deep peak load regulation of power plant [2]; (3) higher cold-end temperature enables the employment of air-cooling which saves water [3, 4].

sCO_2 cycle can be powered by various heat sources, such as nuclear energy, solar energy, fossil fuel, and waste heat [5]. For nuclear and solar energy, the narrow heat source temperature range matches well with the small temperature rise in the heater of sCO_2 cycle, and the recompression cycle (RC) with higher thermal efficiency is considered as the most promising cycle [1, 6]. sCO_2

cycle using fossil fuel energy includes direct-fired open cycle and indirect-fired closed cycle. The Allam cycle is a direct oxy-combustion cycle with high thermal efficiency and full carbon capture [7, 8]. However, combustion under ultra-high pressure and temperature is challenging. Indirect-fired cycle adopts a boiler with heating tubes to separate flue gas and working fluid, which is being developed by France [9, 10], China [11, 12, 13], and Korea [14].

Different from the sCO_2 cycle driven by nuclear energy and solar energy, two key issues emerge when it is used in coal-fired indirect power plants [11]: (1) large pressure drop is caused by the large mass flow rate of sCO_2 in the coal-fired boiler; (2) effective utilization of the medium temperature flue gas heat is challenging. Only a few studies tried to deal with these problems. To reduce the large pressure drop, most studies increased the tube diameters [9, 12, 15]. However, the increased tube diameter is associated with increased tube wall thickness, which causes increased conductive thermal resistance, resulting in safety problems such as overheating. To absorb the heat from medium temperature flue gas, some methods such as adding a low-temperature economizer or bypass flue pipe were proposed [10, 12], but the cycle efficiency was decreased due to the additional heat.

In order to reduce the pressure drop in the sCO_2 boiler, Xu et al. [11] proposed the partial flow strategy which yields boiler module design. For a heating surface in the partial flow mode, both CO_2 flow rate and length were cut to be half of the respective values for conventional flow mode, decreasing the pressure drop to be 1/8 of that in conventional flow mode. The pressure drop of the CO_2 boiler with partial flow mode was shown to be even smaller than that of the supercritical water boiler. The boiler with partial flow mode is different from the conventional water boiler with the once-through cooling wall because both the cooling wall and convective heating surfaces are segmented into several modules, within which the flow rate is half of the total. Thus, the partial flow strategy yields boiler module design, with which the boiler can be called "modular boiler". To recover the residual flue gas heat, the connected-top-bottom-cycle based on cascade energy utilization was presented [16], but with a reduced cycle efficiency due to the efficiency gap between the top and bottom cycles. Therefore, the principle of overlap energy utilization was proposed [17], which maximized the combined cycle efficiency by eliminating the efficiency gap. Furthermore, the components operating in identical CO_2 temperatures and pressures were shared by the top and bottom cycles to simplify the system layout. The system diagram of the 1000 MWe sCO_2 coal-fired power plant based on partial flow strategy, overlap energy utilization principle and component sharing method [17] is described in Section 3.

In boiler design, ensuring the safe operation of the cooling wall is of great importance. This issue is severer in the sCO_2 boiler. On the one hand, the temperature of sCO_2 in the cooling wall is nearly 200°C higher than that of the supercritical water boiler [18] while the main vapor parameters of the sCO_2 boiler (620°C/30 MPa) are equivalent to those of the supercritical water boiler. On the other hand, the convective heat transfer coefficient of sCO_2 in the tube (3000 to 5000 W/(m^2·K)) is lower than that of the supercritical water [19]. Therefore, it is riskier for the sCO_2 cooling wall to be overheated and crack. At present, limited studies have focused on the control of cooling wall temperature of the sCO_2 boiler. Yang et al. [12] obtained the cooling wall temperature distribution for a 300 MWe sCO_2 boiler with a coupled simulation of combustion and fluid heating. Zhou et al. [20] found that the strategies of partial flow mode, flow symmetry, and furnace local expansion reduced the wall temperature and pressure drop effectively. Yang et al. [13] analyzed the 1000 MWe modular sCO_2 boiler and optimized the arrangement of cooling wall modules and concluded that the principle of "cold sCO_2-hot fire matching and cascaded temperature control", combined with counterflow arrangement, can reduce the temperature of the overheated zone by 12°C to 44°C.

The most dangerous heating tube is the one obtaining the maximum wall temperature, and the position of the maximum wall temperature point is regarded as the hot spot. Minimizing the wall temperature of the hot spot is a critical target. In supercritical water boiler design, the heat flux-temperature matching (HTM) method is commonly used to reduce the tube wall temperature [18, 21], which refers to matching the high furnace heat flux with low-temperature water. For example, water with lower temperature is designed to cool the furnace wall while that with higher temperature is arranged in the flue. This method is also useful in the sCO_2 boiler, as shown in Ref. [13], but could fail to obtain the optimal solution for the cooling wall of the modular boiler. That is because the wall temperature is determined not only by heat flux and CO_2 temperature but also by the thermal resistances. The cooling wall in a modular boiler is divided into various modules to heat vapor from the main heater, the first reheater, and the secondary reheater separately. Thus, the convective and conductive thermal resistances are different due to the different thermodynamic states of CO_2 and tube sizes of modules.

In order to achieve the optimal arrangement of the cooling wall modules, the concept of "allowable heat flux" is proposed in this paper, which is the heat flux corresponding to the allowable wall temperature of the

cooling wall tube. The "allowable heat flux" is the upper limit of the heat flux a tube can bear, considering both CO_2 temperature and thermal resistance of a specific module. Based on this concept, the heat flux-heat flux matching (HHM) method, referring to the matching of higher furnace heat flux with higher tube allowable-heat-flux, can further decrease the maximum wall temperature and obtain the optimal scheme and more uniform temperature distribution. Besides, the measures of mid-partition wall, heat transfer enhancement, and downward flow in tubes are comprehensively used based on HHM. It is found that the wall temperature can be further reduced effectively.

This paper is organized as follows. In Section 2, the comparison of HTM and HHM is analyzed. In Section 3, the system diagram of the 1000 MWe sCO_2 coal-fired power plant is introduced. In Section 4, the mathematical model and calculation method are presented and validated. In Section 5, results are reported and analyzed, where Section 5.1 reports the wall temperatures of the cooling wall modules based on HTM and HHM, and Section 5.2 shows the effect of the three temperature control methods. Major conclusions are summarized in the last section.

2. The HTM and HHM methods

Fig. 1 shows the heat transfer model for the membrane cooling wall. The fireside receives radiation heat flux q from the flame, and the other side is insulated. sCO_2 with the temperature of T_f flows in the tubes. The outer wall temperature T_{wo}, inner wall temperature T_{wi}, and fin temperature T_{fin} are shown in the figure. The mean temperature of the tube wall is $T_w=(T_{wo}+T_{wi})/2$.

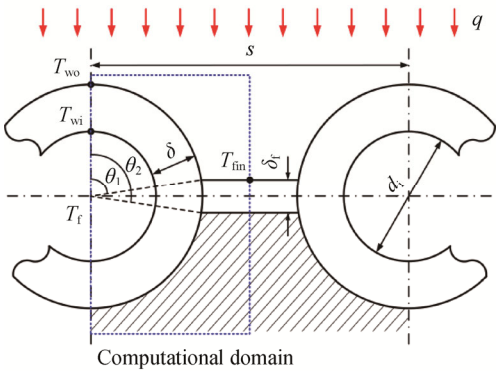

Fig. 1 Two-dimensional heat transfer model for the cooling wall tube

To ensure safety of the tubes, the followed criteria should be satisfied [21]:

$$T_w < T_{w,l} \tag{1}$$

$$T_{wo} < T_{wo,l} \tag{2}$$

$$T_{fin} < T_{wo,l} \tag{3}$$

where $T_{w,l}$ is the temperature limit based on the allowable stress of the tube, regarded as the allowable temperature of the tube related to strength. $T_{wo,l}$ is the allowable temperature of the steel limited by corrosion. For pressure vessels, $T_{w,l}$ is smaller than $T_{wo,l}$.

Based on classical heat transfer solution, the mean wall temperature can be expressed as [21, 22]:

$$T_w = T_f + \Delta T_w = T_f + Cq \tag{4}$$

$$C = \mu\beta\left[\frac{1}{\alpha_f} + \frac{\delta}{\lambda(\beta+1)}\right] \tag{5}$$

where the coefficient C can be considered as a comprehensive thermal resistance, directly related to the convective thermal resistance $1/\alpha_f$, the conductive thermal resistance $\delta/[\lambda(\beta+1)]$, and the mean heat distribution coefficient at the center of the fireside tube wall μ. δ, β and λ are tube wall thickness, the ratio of outer diameter to inner diameter, and thermal conductivity, respectively. μ is the ratio of the heat transfer rate for non-uniform circumferential heating to that for uniform circumferential heating at the maximum heat flux point, which is a function of β, pitch-diameter ratio s/d_o and Biot number Bi.

Assume there are two domains in the boiler with different heat fluxes dominated by different flue gas temperatures, and two heating modules, Module 1 with lower T_f and Module 2 with higher T_f, as shown in Fig. 2(a) and Fig. 2(b). According to the HTM method, Module 1 and Module 2 are matched with high q and low q respectively to reduce the tube wall temperatures. When the two modules have identical C, T_w is only determined by T_f and q according to Eq. (4), thus optimal wall temperature distribution is obtained, as shown in Fig. 2(c). However, when C_1 is larger than C_2, the effect of the temperature difference $\Delta T_w=Cq$ in Eq. (4) may be larger than that of T_f on T_w. As a result, Module 1 has a higher T_w and can even be overheated, as shown in the shaded area of Fig. 2(d). Therefore, T_w depends not only on T_f and q but also on the comprehensive thermal resistance C. HTM method is effective when the difference of C is negligible among various modules, but it is not applicable when the difference is large enough to change the trend. This phenomenon inspired us to consider the new parameter "allowable heat flux" containing T_f and C to match with the local heat flux.

As a principle, $T_w<T_{w,l}$ should be satisfied, shown in Fig. 2(e). The "allowable heat flux" is the heat flux that obtains $T_w=T_{w,l}$ for the tube, which can be written from Eqs. (4) and (5) as:

$$q_l = \frac{T_{w,l} - T_f}{C} = \frac{T_{w,l} - T_f}{\mu\beta\left[\frac{1}{\alpha_f} + \frac{\delta}{\lambda(\beta+1)}\right]} \quad (6)$$

Therefore, q_l along the tube is the maximum heat flux the tube can bear. Based on this concept, the criterion of temperatures in Eq. (1) can be converted into that of heat fluxes as:

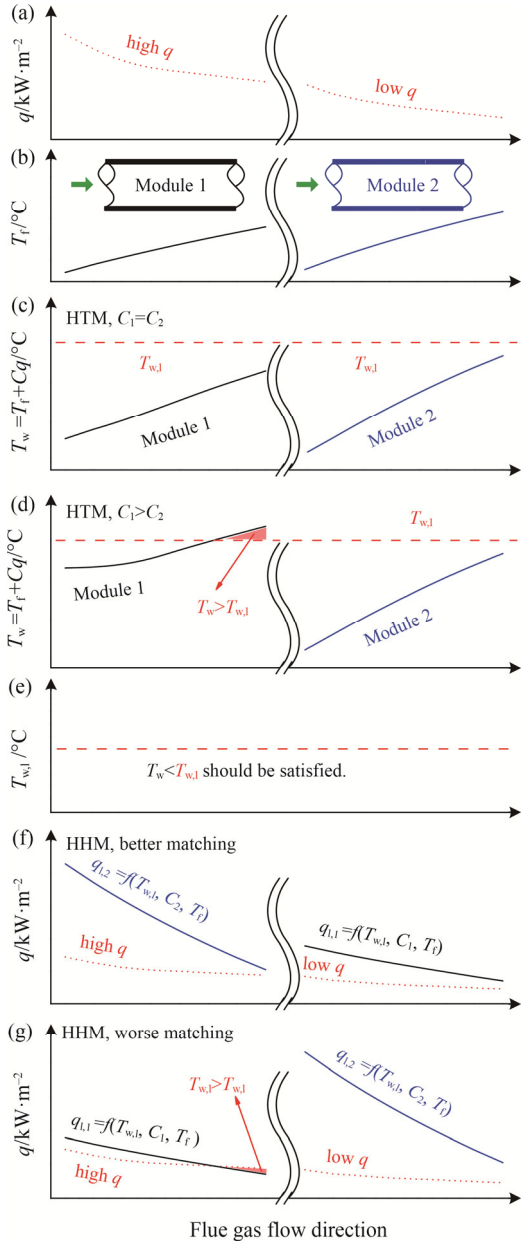

Fig. 2 Comparison of mechanisms between HTM and HHM (a): heat flux distribution, (b): T_f of two modules, (c): $T_{w,l}$, (d): HTM method with C_1=C_2, (e): HTM method with C_1>C_2, (f): better HHM matching of higher q_l versus higher q, (g): worse HHM matching of lower q_l versus higher q.

$$q_l > q \quad (7)$$

Provided the allowable heat flux is higher than the local heat flux, the cooling wall is safe. Thus, HHM method locates the modules with high allowable heat flux at the area of high local heat flux.

Fig. 2(f) and 2(g) show the better and worse matching based on HHM method respectively. Module 1 gets lower q_l due to the higher C_1, while Module 2 yields higher q_l. When Module 1 is matched with high heat flux, an overlapping zone emerges as shown in Fig. 2(g), where q_l is smaller than q, corresponding to the shaded area in Fig. 2(d).

The HHM brings the comprehensive thermal resistance C into matching design, improving the HTM method by eliminating the potential errors caused by different C. The HHM method provides a new simple matching principle for boiler design, especially for the modular boiler.

3. Thermal Power System

Fig. 3 shows the system diagram of the 1000 MWe sCO_2 coal-fired power plant proposed by Sun et al. [17]. Based on the combined cycle, overlap energy utilization principle, and component sharing method, the system eliminates the efficiency gap between the top and bottom cycle, providing an effective way to utilize the flue gas heat. Both the top and bottom cycles are recompression cycles with double reheating. The power system consists of three turbines (T1, T2, T3) to drive generators, three recuperators (HTR1, HTR2, LTR) to recycle heat, two compressors (C1, C2) to elevate the pressure, a cooler to dissipate extra heat, an external air preheater (EAP) to recycle heat for the bottom cycle, and a boiler (including 13 heat exchanger modules and an AE) to drive the cycle. The power generation efficiency reaches 47.99% at the main vapor parameters of 620°C/30 MPa [17], higher than that of the most advanced supercritical steam cycle.

For the same heat load, partial flow strategy separates the CO_2 flow rate into two halves, and the heating length is also decreased to be half. Hence, the friction pressure drop is reduced to 1/8 since it is scaled as ΔP_f–$m^2 l$. Partial flow mode yields boiler module design, as shown in Fig. 3. The mainstream, first reheating stream, and second reheating stream are separated into two parallel lines respectively. Module 1 and Module 2 of the main heater, Module 3 of the first reheater, and Module 4 of the second reheater are located in the furnace as cooling wall, as shown in the black dashed frame. The operation parameters of the four modules are listed in Table 1. This paper is aimed at arranging the four modules to achieve the minimum wall temperature at the hot spot.

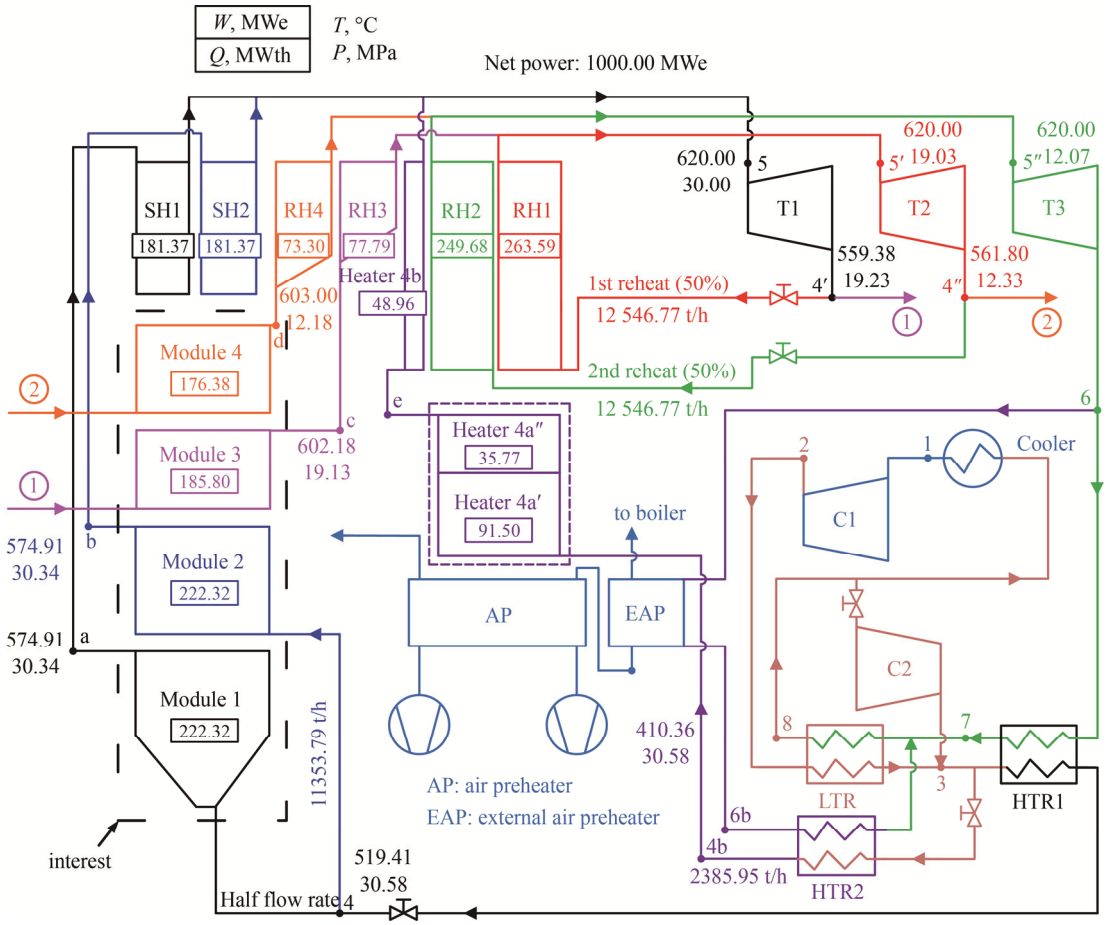

Fig. 3 The 1000 MWe sCO_2 coal-fired power plant design proposed by Sun et al. [17]

Table 1 Cooling wall parameters of the 1000 MWe sCO_2 boiler

		Temperature/°C	Pressure/MPa	Mass flow rate/t·h^{-1}	Thermal load/MWth
Module 1	Inlet	519.41	30.58	11 353.79	222.32
	Outlet	574.91	30.34	11 353.79	
Module 2	Inlet	519.41	30.58	11 353.79	222.32
	Outlet	574.91	30.34	11 353.79	
Module 3	Inlet	559.38	19.23	12 546.77	185.80
	Outlet	602.18	19.13	12 546.77	
Module 4	Inlet	561.80	12.33	12 546.77	176.38
	Outlet	603.00	12.18	12 546.77	

4. Model and Methods

Numerical heat transfer models are developed based on the one/two-dimensional model of the conjugate heat transfer [23, 24] for the cooling wall. The one-dimensional model is used to calculate the sCO_2 thermal parameters along the tube axial direction under the preset heat flux condition, and the two-dimensional model is applied to simulate the heat transfer on the cross-section of the cooling wall tube using the finite-volume method to solve the temperature distribution [25]. The assumptions in this work are given as follows,

(1) The non-uniformity of heat flux along the furnace circumference is neglected, but the angle coefficients of the tube wall and fin are considered in the two-dimensional model.

(2) The mass flow rate of sCO_2 distributes uniformly in the tubes.

(3) The axial heat transfer in the tube wall is neglected.

(4) The physical properties of sCO_2 remain constant in

the cross-section of the tube.

(5) Heat loss from the furnace wall to the environment is neglected.

4.1 Numerical model

A Pi-type boiler with eight-square two-tangential firing is applied as the 1000 MWe sCO_2 boiler in Fig. 3. The vertical smooth tube is used for the sCO_2 membrane cooling wall. The geometry of the boiler and the distribution of heat flux non-uniformity coefficient along its height are shown in Fig. 4.

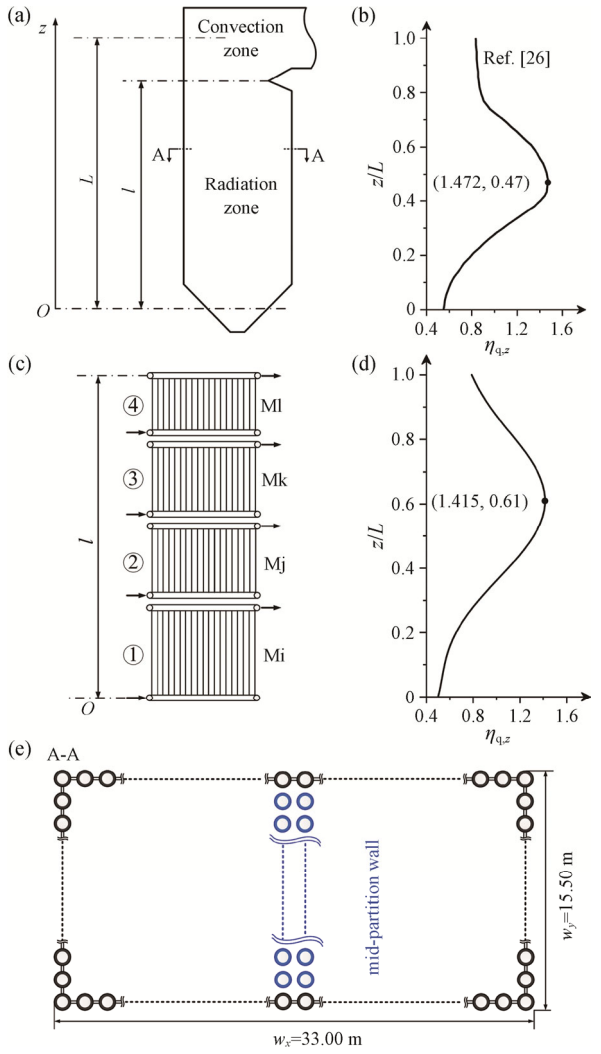

Fig. 4 Numerical model for the cooling wall (a): geometry of the furnace, (b): heat flux non-uniformity coefficient along the furnace height, (c): geometry of the cooling wall, (d): heat flux non-uniformity coefficient along the cooling wall height, (e): membrane cooling wall in furnace cross-section.

The heat flux non-uniformity coefficient is defined as the ratio of the local heat flux to the average heat flux in the furnace. The furnace hopper center is set as the baseline. L and l correspond to the height from the baseline to the furnace exit center and the furnace arch center, respectively. Fig. 4(b) shows the distribution of the heat flux non-uniformity coefficient along with the height of L in a typical ultra-supercritical boiler [26], while Fig. 4(d) shows that of l, which is the total height of Modules 1–4 given in Fig. 4(c). The local heat flux non-uniformity coefficient is decreased as the low-heat flux part from l to L is excluded during the calculation. Since the average heat flux of the whole water wall in the water-steam boiler is usually below 130 kW/m^2 [18], it is set as 144 kW/m^2 in the present work. Fig. 4(e) shows the dimensions of a furnace cross-section. The width is 33 m and the depth is 16.5 m. The dimensions are equivalent to those of the 1000 MWe ultra-supercritical water boiler.

4.2 One-dimensional heat transfer model

The one-dimensional model is developed to describe the flow and heat transfer process of sCO_2 in the tube. The conservation equations of mass, momentum, and energy are given as follows [23]:

$$\frac{\mathrm{d}m}{\mathrm{d}z}=0 \tag{8}$$

$$\frac{\mathrm{d}P}{\mathrm{d}z}+\frac{\mathrm{d}P_\mathrm{f}}{\mathrm{d}z}+\frac{m^2}{A^2}\frac{\mathrm{d}}{\mathrm{d}z}\left(\frac{1}{\rho}\right)+\rho g=0 \tag{9}$$

$$\frac{\mathrm{d}h}{\mathrm{d}z}=q_z\frac{s}{m} \tag{10}$$

where m is the mass flow rate of sCO_2 in a single tube, $m=M/n$. A is the cross-sectional area per tube. q_z is the local heat flux at the height of z, which can be derived with the non-uniformity coefficient in Fig. 4(d), $q_z=q_{\mathrm{ave}}\eta_{\mathrm{q},z}$. The pressure drop caused by friction, $\mathrm{d}P_f$, is given by the Darcy-Weisbach expression [27]:

$$\mathrm{d}P_f=f\frac{\rho u^2}{2}\frac{\mathrm{d}z}{d_\mathrm{i}} \tag{11}$$

where f is obtained from the Filonenko equation [28]:

$$f=\frac{1}{1.821\mathrm{g}(Re)-1.64} \tag{12}$$

According to the heat loads of Modules 1–4 in Fig. 3, the height of each module can be calculated by:

$$Q_i=\int_{l_{i-1}}^{l_i}2\left(w_x+w_y\right)q_z\mathrm{d}z \tag{13}$$

4.3 Two-dimensional heat transfer model

A two-dimensional heat conductive model is built to obtain the temperature distribution in the tube wall and the fin. Corresponding to the computational domain shown in the dashed frame of Fig. 1, the governing equations are given as follows [25]:

$$\frac{\partial}{\partial r}\left(r\lambda\frac{\partial T}{\partial r}\right)+\frac{\partial}{\partial\theta}\left(\frac{\lambda}{r}\frac{\partial T}{\partial\theta}\right)=0 \tag{14}$$

$$\frac{\partial}{\partial x}\left(\lambda\frac{\partial T}{\partial x}\right)+\frac{\partial}{\partial y}\left(\lambda\frac{\partial T}{\partial y}\right)=0 \tag{15}$$

Here, Eq. (14) is based on cylindrical coordinates while Eq. (15) is based on Cartesian coordinate. The block-structured grid is used to mesh the computational domain, and the decomposition method is applied to transfer information between the overlapped grids. The angle coefficients of the tube wall and fin on the fireside are obtained by the method of cross-line [29]. Other details about the boundary conditions are listed in Table 2.

Table 2 Boundary conditions in the two-dimensional model

Components	Boundary conditions
Tube wall	$-\lambda\left.\frac{\partial T}{\partial r}\right\|_{r=r_i}=\alpha_f(T-T_f)$, $-\lambda\left.\frac{\partial T}{\partial r}\right\|_{r=r_o,0\le\theta\le\theta_1}=q\cdot\varphi_\theta$
	$T\left\|_{r=r_o,\theta_1\le\theta\le\theta_2}=T_{interface}\right.$, $-\lambda\left.\frac{\partial T}{\partial r}\right\|_{r=r_o,\theta_2\le\theta\le\pi}=0$
Fin	$-\lambda\left.\frac{\partial T}{\partial r}\right\|_{y=\delta_f/2}=q\cdot\varphi_x$, $-\lambda\left.\frac{\partial T}{\partial r}\right\|_{y=-\delta_f/2}=0$

The state of sCO_2 in Modules 1–4 is far from the pseudo-critical point, presented by the dashed lines in Fig. 5. In this regime, the Dittus-Boelter correlation has a relatively high precision for the prediction of in-tube convective heat transfer coefficient for supercritical water and sCO_2 [30–32]. Hence, it is employed to predict the in-tube heat transfer coefficient of sCO_2:

$$\alpha_f=0.023\frac{\lambda_f}{d_i}Re_f^{0.8}Pr_f^{0.4} \tag{16}$$

where λ_f is the thermal conductivity of sCO_2; Re_f and Pr_f are the Reynolds number and Prandtl number of sCO_2 respectively.

The one-dimensional and two-dimensional models are developed in the Matlab environment. The physical properties of sCO_2 are obtained from the database REFPROP 9.1 [33].

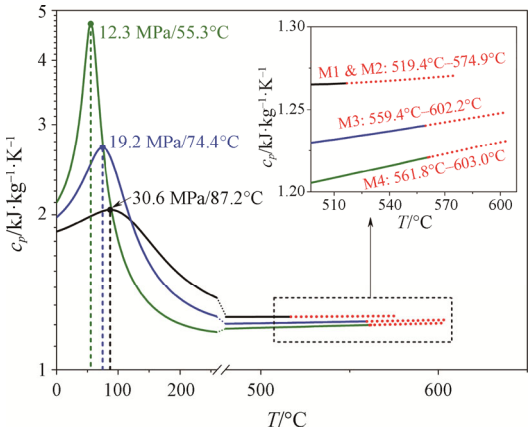

Fig. 5 The state of sCO_2 in Modules 1–4 that far from the pseudo-critical point

4.4 Material and dimensions of the tube and fin

The maximum temperature of the sCO_2 cooling wall approaches 700°C, and Super 304H (10Cr18Ni9NbCu3BN) is thus selected as the material for the cooling wall tube and fin [34]. The thickness of the tube wall can be determined by [35]:

$$\delta=\frac{Pd_i}{2\varphi_{min}[\sigma]-P}+c \tag{17}$$

where φ_{min} is the minimum reduction factor and is set as 1.0; c is the additional thickness and is set as 1.0 mm; $[\sigma]$ is the allowable stress of the tube wall under $T_{w,l}$. The $T_{w,l}$ of the tubes in Module 1–4 is evaluated as 650°C in the present work. Consequently, the allowable stress of the Super 304H is 78 MPa.

Parameters for other sizes are then determined and shown in Table 3. Structures 1 and 2 correspond to arrangements of the cooling wall without and with the mid-partition wall, respectively, as shown in Fig. 4(e).

4.5 Model validation

The one- and two-dimensional models are validated by the data from a supercritical steam boiler in Zima

Table 3 Structural parameters of the cooling wall

		Unit	Module 1	Module 2	Module 3	Module 4
Structure 1	$d_i\times\delta$	mm×mm	23.0×6.6	23.0×6.6	30.0×5.4	30.0×3.7
	d_o	mm	36.2	36.2	40.8	37.4
	s	mm	45.3	45.3	51.0	46.8
	n	/	2185	2185	1941	2115
	δ_f	mm	6.0	6.0	6.0	6.0
Structure 2 (with mid-partition wall)	$d_i\times\delta$	mm×mm	20.0×6.0	20.0×6.0	26.0×4.8	26.0×3.4
	d_o	mm	32.0	32.0	35.6	32.8
	s	mm	41.6	41.6	46.3	42.6
	n	/	3170	3170	2846	3093
	δ_f	mm	6.0	6.0	6.0	6.0

et al. [36] due to the lack of data for the sCO_2 cooling wall. The main vapor parameter is 26 MPa/554°C and the mass flow rate is 2400 t/h. The tube size $d_o \times \delta$ is 33.7 mm× 6.3 mm below 49.4 m and 38.0 mm×6.3 mm above 49.4 m.

The temperature distribution is obtained by the present models and shown in Fig. 6. It can be seen that the modeling results agree well with the data from Zima et al. [36]. The maximum error of temperature is 0.97%. Thus, the present models are precise enough to study the temperature distribution of the sCO_2 cooling wall.

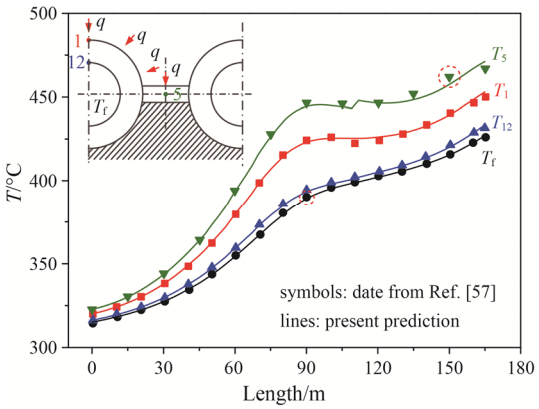

Fig. 6 Validation of the numerical model

5. Results and Discussion

5.1 Arrangement of Modules 1–4 based on the HHM method

Fig. 7 shows the results of optimal arrangements according to HTM and HHM methods, 3124 in Fig. 7(a) and 4123 in Fig. 7(b), respectively. The number 3124 represents the module arrangement of M3-M1-M2-M4 from the bottom upwards. According to Eqs. (1)–(3), three wall temperatures are concerned and calculated: the mean wall temperature T_w, outer wall temperature T_{wo}, and fin temperature T_{fin}. The sCO_2 flows upwards in the tube, and thus the highest wall temperatures appear at the outlets of the tubes for each module. The points obtaining the maximum T_w or T_{wo} among the modules are hot spots that should be paid more attention to, such as the outlets of M3 and M1 in Fig. 7(a) marked by dashed circles. The local heat flux at the outlets of the modules is in the order of $q_a<q_b<q_c<q_d$, as shown by the black dots which are the same as that in Fig. 4(d).

The outlet temperatures of Modules 1–4 are 574.9°C, 574.9°C, 602.2°C, and 603.0°C respectively, and thus the optimal arrangement of 3124 by HTM method can be obtained. However, the coefficient C varies widely among the modules, represented by the dashed blue lines in Fig. 7(a). The higher C of M3 leads to higher temperature rise $\Delta T_w=Cq$, which is 52.69°C at the outlet and is 13.56°C higher than that of M4 in Fig. 7(a). Consequently, M3 has a higher T_w of 654.89°C. In contrast, the arrangement of 4123 in Fig. 7(b) obtains $\Delta T_w=Cq$=46.30°C at the outlet of M4, lower than that of M3 in Fig. 7(a), and a lower T_w of 649.31°C is achieved, meeting the stress requirement of the tube.

The allowable heat fluxes of each module calculated from the parameters in Table 1 and Table 3 are shown in Fig. 7(b) marked by q_l, with dots at the outlets: $q_{l,M1out}=q_{l,M2out}$=206.29 kW/m^2, $q_{l,M3out}$=125.50 kW/m^2, and $q_{l,M4out}$=137.18 kW/m^2. According to the HHM method, Module 3 with the lowest q_l should be installed in the area with the lowest local heat flux. Hence the optimal arrangement as 4123 can be directly achieved. The heat flux allowance at the outlet of the modules, defined as $\Delta_i=q_{l,Miout}-q_{Miout}$, is shown in Fig. 7(b): Δ_4=2.62 kW/m^2, Δ_1=4.89 kW/m^2, Δ_2=28.77 kW/m^2, Δ_3=11.89 kW/m^2. Δ_4 is close to zero, indicating that T_w at the outlet of M4 is very close to $T_{w,l}$. Fig. 8 shows the temperature distribution of the tube wall at the outlet of M1. The maximum T_{wo} at the outlet of M1 is 25.7°C lower than $T_{wo,l}$. The maximum temperature in the fin is much lower than that of the tube.

From Figs. (7)–(8), the HHM method is proved to be effective for the arrangement of cooling wall modules in the 1000 MWe boiler. If the HHM method is not used, the cooling wall tube would have the risk of overheating. Fig. 9 shows the temperature distribution of an arrangement as 1342, which is carried out in an opposite approach of the HHM. It is clear that the tubes at the outlet of M3 and M4 are overheated. The highest T_w and T_{wo} both appear in M3. $T_{w,max}$ is 28.45°C higher than $T_{w,l}$, and $T_{wo,max}$ is only 2.14°C lower than $T_{wo,l}$. Fig. 10 shows the comparison of the optimal arrangement as 4123 and the worst arrangement as 1342. In Fig. 10(a), all the q_l curves are above the q curves, and the heat flux differences are relatively uniform. In contrast, a crossover of q_l and q curves occurs in M3 and M4 in Fig. 10(b), indicating that those tubes from the intersection to the outlet are all overheated. Meanwhile, significant non-uniform heat flux differences exhibit in M1 and M2. Therefore, the HHM method makes the wall temperature distribution relatively uniform, reducing the thermal stress of the cooling wall consequently.

The allowable heat flux of the module represents the ability of the module to bear the furnace heat flux. The optimal matching between allowable heat flux and local heat flux makes the best of this ability to obtain a more uniform heat flux allowance and wall temperature. Theoretically, when the number of modules approaches infinity, the minimum wall temperature of the whole cooling wall will be obtained. The HHM method is an

effective matching strategy to achieve the lowest hot spot temperature of the cooling wall tubes.

5.2 Measures guided by HHM to reduce the tube wall temperature

The results in Figs. 7 and 8 show that the mean tube wall temperature of the sCO_2 cooling wall is still relatively high even at the optimal arrangement of 4123, only 0.7°C lower than the allowable wall temperature. Thus, it is necessary to reduce the tube wall temperature further. The HHM method shows that a higher heat flux allowance at the outlet of module Δ_i yields a lower wall temperature. Thus, raising the Δ_i can decrease the wall temperature. The Δ_i can be rewritten as:

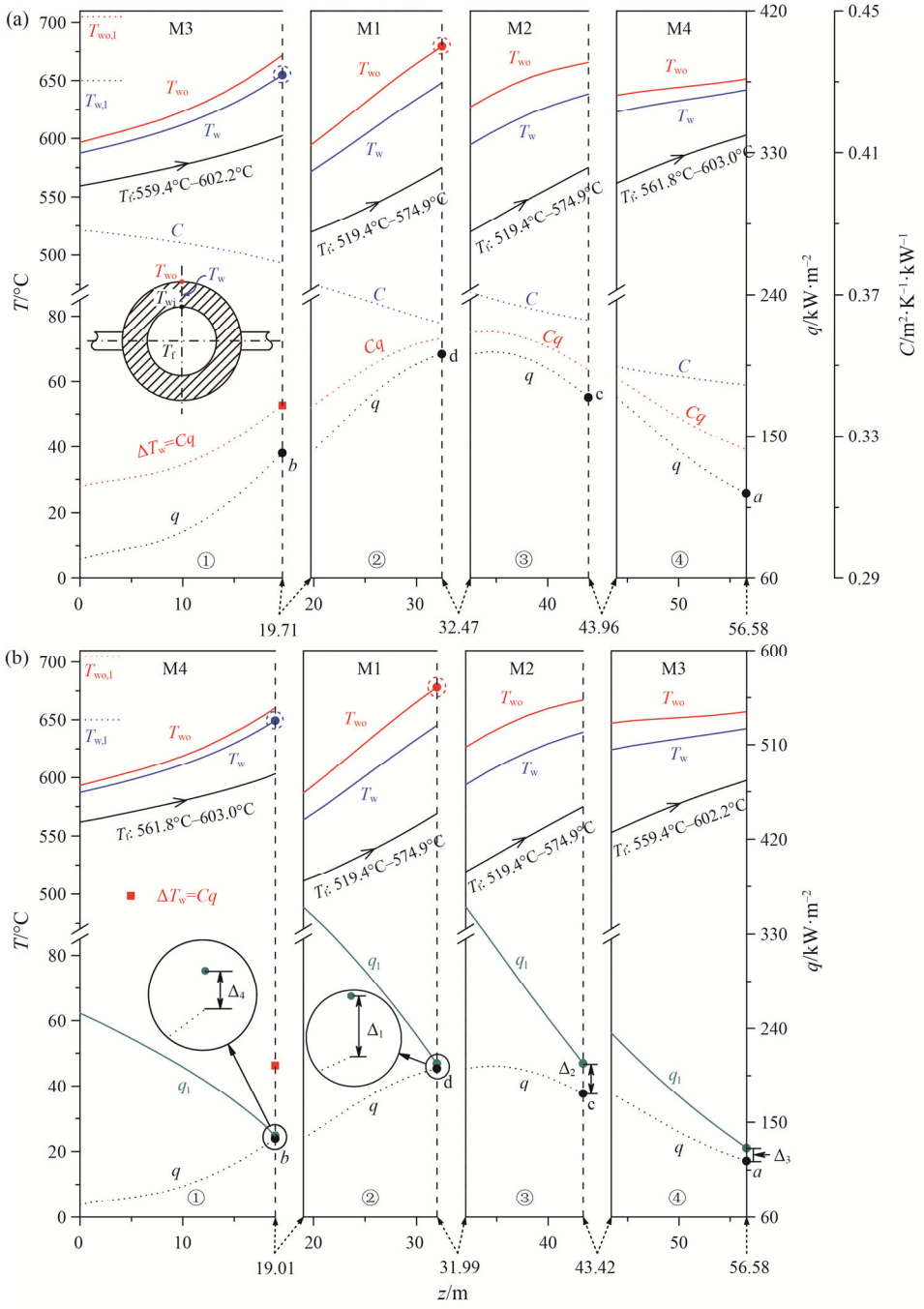

Fig. 7 Comparison of optimal arrangements according to the HTM and HHM method (q_a<q_b<q_c<q_d, $T_{wo,l}$=705.0°C, $T_{w,l}$= 650.0°C; a: optimal arrangement of 3124 based on HTM, $T_{wo,max}$ =679.68°C, $T_{w,max}$ =654.89°C, $\Delta T_{w,M3out}$=52.69°C; b: optimal arrangement of 4123 based on HHM, $T_{wo,max}$=679.26°C, $T_{w,max}$=649.31°C).

$$\Delta_i = q_{\mathrm{l,Miout}} - q_{\mathrm{Miout}} = \left(\frac{T_{\mathrm{w,l}} - T_{\mathrm{f}}}{C}\right)_{\mathrm{Miout}} - q_{\mathrm{Miout}} \quad (18)$$

Eq. (18) shows that decreasing the local heat flux q_{Miout} or increasing the allowable heat flux $q_{\mathrm{l,Miout}}$ are possible approaches. The former can be achieved by adding a mid-partition wall or applying downward flow in the tube, and the latter can be achieved by reducing the thermal resistances. The results of these methods are discussed in this section.

5.2.1 Adding the mid-partition wall

The mid-partition wall in a furnace is sometimes used as an additional heating surface in large-scale boilers [21, 37]. In the present work, it is employed because the average heat flux can be reduced with the increased heat transfer area, as shown in Fig. 4(e). The vertical smooth tube without fins is used for the mid-partition wall and the structure parameters are given in Table 3. A smaller inner diameter is selected as more tubes are used. Fig. 11 shows the temperature distribution of the modules arranged as 4123. The average heat flux is the ratio of heat load to heat transfer area in the furnace. The heat load is assumed to be constant due to the constant flue gas temperature at the furnace outlet. For the mid-partition wall, the fireside receives radiation heat flux and the other side is assumed to be insulated. The heat transfer area is $A_{\mathrm{furnace}}=2l(w_x+w_y)$ and $A_{\mathrm{furnace,mid}}=l[2(w_x+w_y)+2w_y)]$ for furnace without and with mid-partition wall, respectively, as shown in Fig. 4(e). Due to the relationship of $w_x=2w_y$, it can be obtained that the latter is 4/3 of the former. Thus the average heat flux is reduced to 3/4 of the original value, from 144 kW/m^2 to 108 kW/m^2. Hence, the heat flux along the height drops down, especially in the peak region. Meanwhile, the allowable heat fluxes based on the parameters of Structure 2 in Table 3 just change a little compared with Structure 1. Therefore, the heat flux allowances are increased significantly to be Δ_4=32.38 kW/m^2, Δ_1=54.49 kW/m^2, Δ_2=72.41 kW/m^2, and Δ_3=39.58 kW/m^2. Thus, the mean wall temperatures and outer wall temperatures are all reduced by a large extent. The maximum mean wall temperature is 638.40°C at the outlet of M4, 10.91°C lower than that without mid-partition wall as shown in Fig. 7(b).

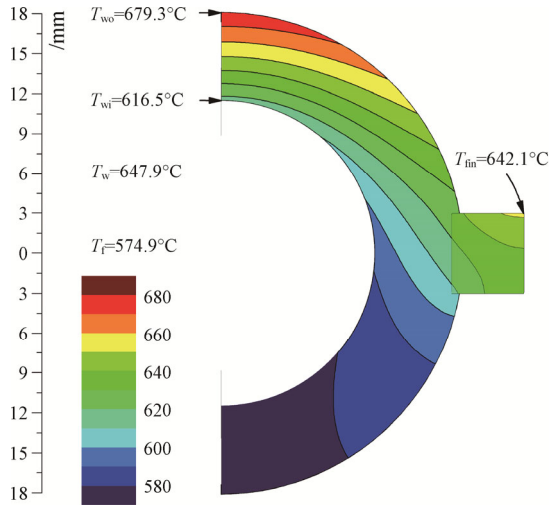

Fig. 8 Temperature distributions at the outlet of M1 under the optimal arrangement (4123)

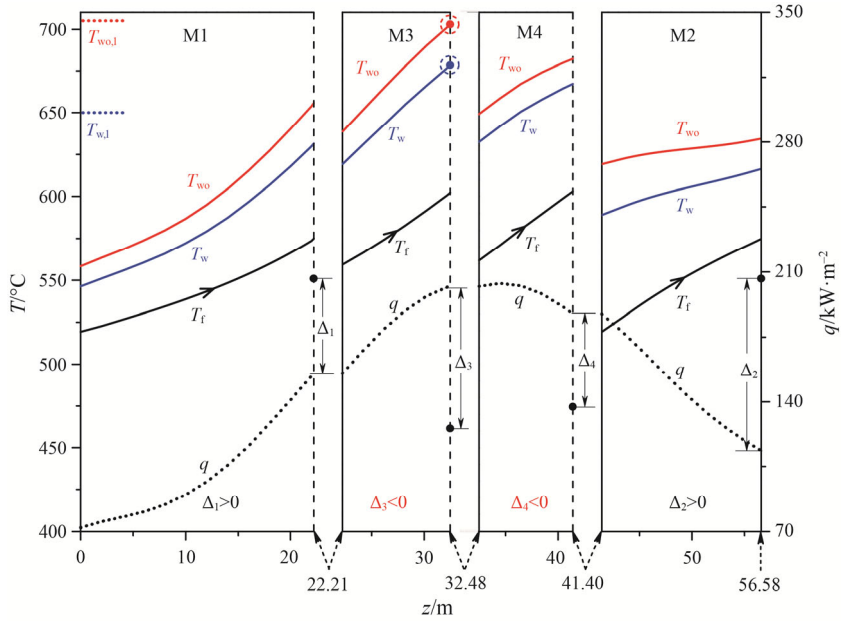

Fig. 9 Wall temperatures of the converse arrangement (1342) based on HHM ($T_{\mathrm{wo,max}}$=702.86°C, $T_{\mathrm{w,max}}$=678.45°C)

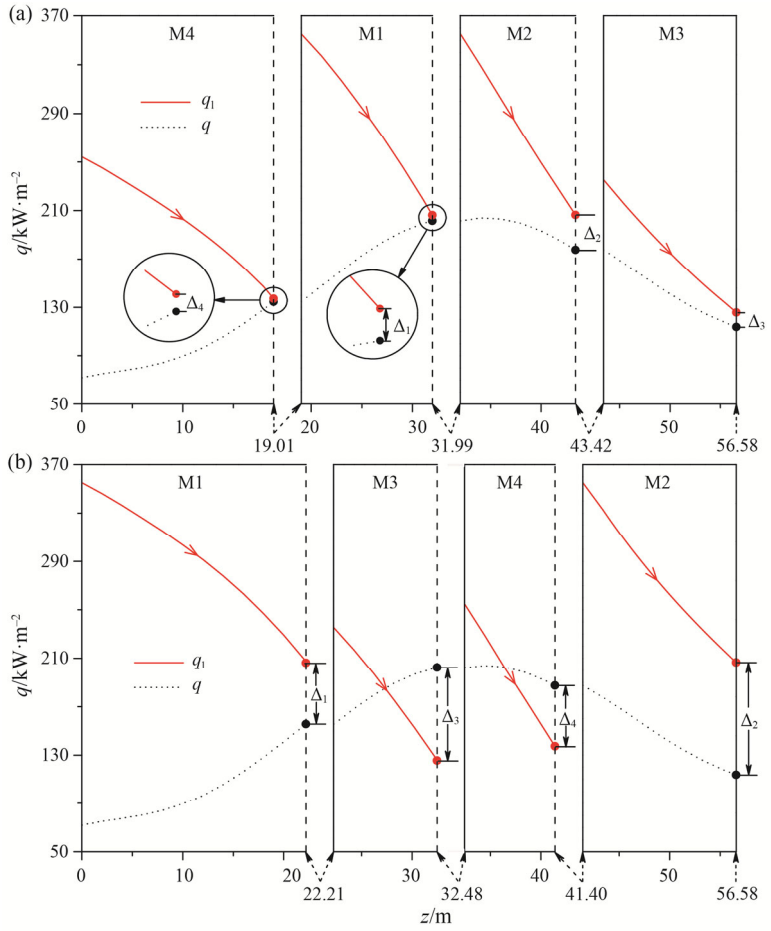

Fig. 10 Matching analysis between allowable heat flux and local heat flux under the optimal and worst arrangement ((a): arrangement of 4123; (b): arrangement of 1342)

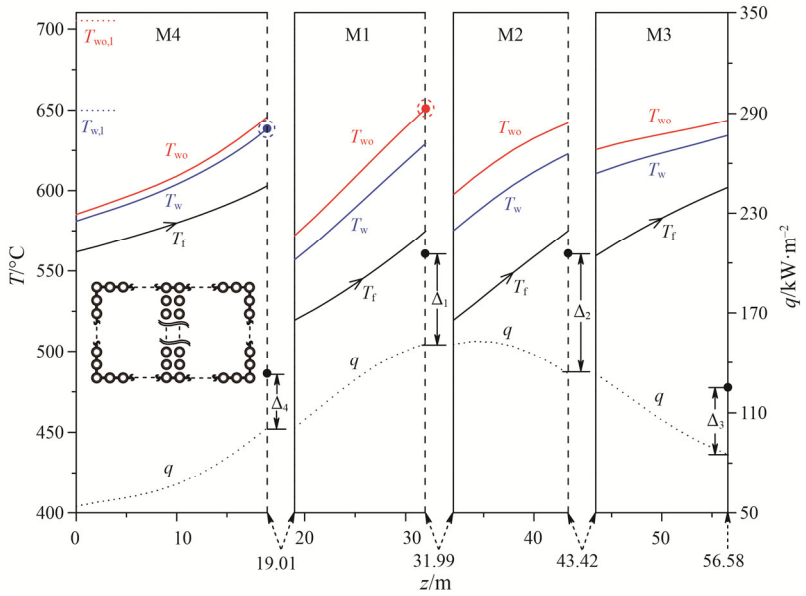

Fig. 11 Temperatures of modules with mid-partition wall under the optimal arrangement (4123)($T_{wo,max}$ =651.12°C, $T_{w,max}$ = 638.40°C; $q_{l,M4out}$=133.38 kW/m^2, $q_{l,M1out}$ =$q_{l,M2out}$ =205.66 kW/m^2, $q_{l,M3out}$=124.86 kW/m^2)

5.2.2 In-tube convective heat transfer enhancement

Fig. 12 shows the distribution of the thermal resistance through the tube wall, including the conductive thermal resistance $R_{cd}=\delta/[\lambda(\beta+1)]$, the convective thermal resistance $R_{cv}=1/\alpha_f$, and ratio=$R_{cv}/(R_{cv}+R_{cd})$. It can be seen that the convective thermal resistance contributes to most of the total thermal resistance. Thus, enhancement of the in-tube convective heat transfer is an effective way to reduce the tube wall temperature.

The in-tube heat transfer enhancement techniques have been widely studied, such as internally rifled tubes, dimpled tubes, and helical coiled tubes [38, 39]. The rifled tubes are widely used in the water-steam boiler to delay heat transfer deterioration [18]. However, the heat transfer in sCO_2 boiler falls into the normal heat transfer regime which is far from the pseudo-critical regime due to the high temperature of sCO_2. Limited corrections can be found concerning the enhanced heat transfer coefficients for this regime. Hence, in this paper, we increase the convective heat transfer coefficient to 1.5 times of the original value to explore its potential for decreasing the tube wall temperature, providing a reference for further studies. Fig. 13 shows the temperature distribution with both the mid-partition wall and the enhanced tubes. Compared with those in Fig. 11, $q_{l,Miout}$ is increased by 20%–35%, and Δ_i is increased by 65%–150%. The maximum mean wall temperature T_w still appears at the outlet of M4, and is further reduced by 8.77°C, from 638.40°C to 629.63°C. The maximum outer wall temperature T_{wo} is decreased by 9.51°C, from 651.12°C to 641.61°C.

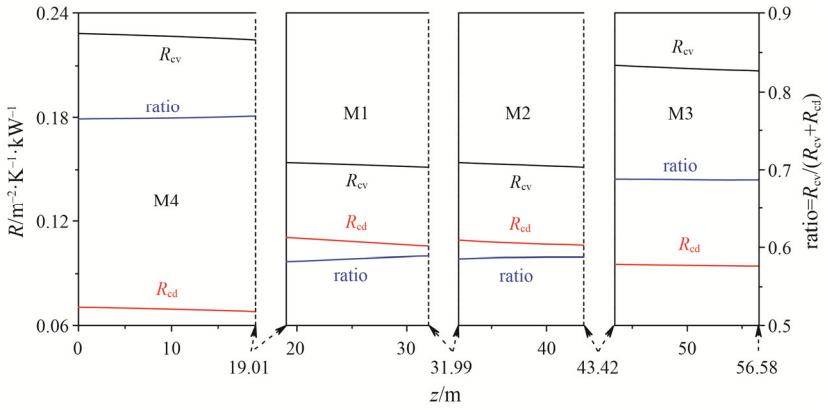

Fig. 12 Thermal resistance of the tube wall under the optimal arrangement (4123)

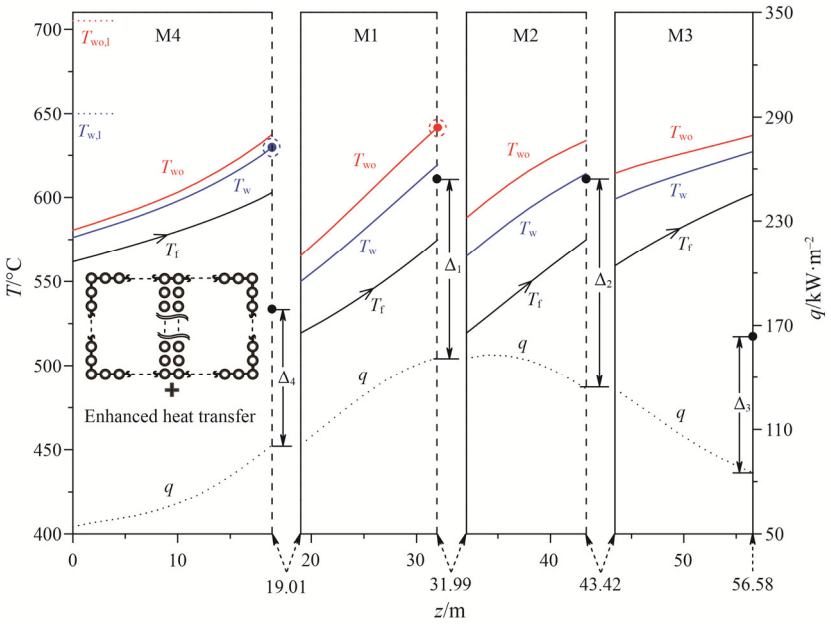

Fig. 13 Temperatures of modules with mid-partition wall and enhanced heat transfer under the optimal arrangement (4123) ($\alpha_{f,e}$=1.5α_f, $T_{wo,max}$ =641.61°C, $T_{w,max}$ =629.63°C, $q_{l,M4out}$ =179.30 kW/m^2, $q_{l,M1out}$ =$q_{l,M2out}$ =254.18 kW/m^2, $q_{l,M3out}$ =163.61 kW/m^2)

5.2.3 Application of the downward flow

Fig. 14(a) shows the matching between q_l and q of the modules with sCO_2 flowing upwards. According to the definition of q_l in Eq. (6) and Fig. 14(a), q_l decreases with the increase of T_f and reaches the minimum at the outlet of the module. However, the local heat flux at the lower part of the furnace rises with height, attaining the maximum within a module at the outlet, as shown in Module 4 and Module 1 in Fig. 14(a). As a result, within the module, higher q_l matches with lower q, and lower q_l matches with higher q, suppressing the heat flux allowance to a small value. The downward flow can change this situation, which is shown in Fig. 14(b). With the downward flow employed in Module 4 and Module 1, the local heat flux at the outlet becomes the minimum within the module. This significantly elevates Δ_4 and Δ_1 from 78.30 kW/m^2 to 125.32 kW/m^2 and 103.01 kW/m^2 to 153.76 kW/m^2, respectively.

Fig. 15 shows the distribution of temperatures in modules corresponding to Fig. 14(b). The reduced Δ_4 and Δ_1 significantly decrease the wall temperature in Module 4 and Module 1. T_w at the outlet of Module 4 is decreased from 629.63°C to 617.13°C, and T_{wo} at the outlet of Module 1 is decreased from 641.61°C to 619.59°C, which are much lower than those of the other two modules. Thus, the locations of the maximum T_w and T_{wo} are changed from the outlet of Module 4 to that of Module 3. The maximum T_w and T_{wo} are 627.23°C and 636.74°C, which are 2.40°C and 4.87°C lower than those shown in Fig. 13, respectively.

With the application of the downward flow, it is noted that the range of local heat flux at the module outlets is changed to $q_{M4out}<q_{M3out}<q_{M1out}<q_{M2out}$. However, the range of the allowable heat flux remains the same: $q_{l,M3out}<q_{l,M4out}<q_{l,M1out}=q_{l,M2out}$. Hence, the arrangement of the modules is further optimized from 4123 to 3124 according to the HHM method. Figure 16 shows the temperature distribution in the modules with the arrangement as 3124. It can be seen that the maximum mean wall temperature of 625.43°C appears at the outlet of M4, which is 1.80°C lower than that in the arrangement of 4123, and the maximum outer wall temperature of 632.83°C appears at the outlet of M2, 3.91°C lower than that in the arrangement of 4123.

The $T_{w,max}$ and $T_{wo,max}$ under different module arrangement and optimization measures are summarized in Table 4. Under the constraint of $T_{wo,l}$=705.0°C and $T_{w,l}$=650.0°C, the worst arrangement of 1342 cannot satisfy the criterion in Eq. (1) as $T_{w,max}$ (678.45°C) is higher than $T_{w,l}$. With the improvement in the module arrangement and the optimization measures, $T_{wo,max}$ and $T_{w,max}$ keep decreasing.

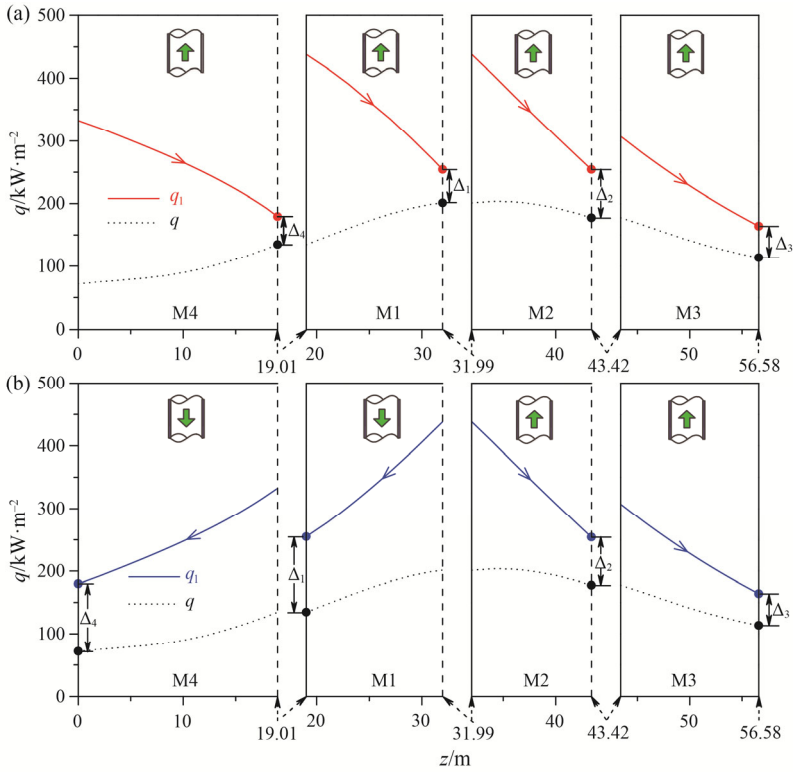

Fig. 14 Matching analysis between q_l and q of the modules with mid-partition wall and enhanced heat transfer under the optimal arrangement (4123) ($\alpha_{f,e}$=1.5α_f ; $q_{l,M4out}$=179.30 kW/m^2, $q_{l,M1out}$ = $q_{l,M2out}$ =254.18 kW/m^2, $q_{l,M3out}$=163.61 kW/m^2; a: M1 and M4 flows upwards; b: M1 and M4 flows downwards)

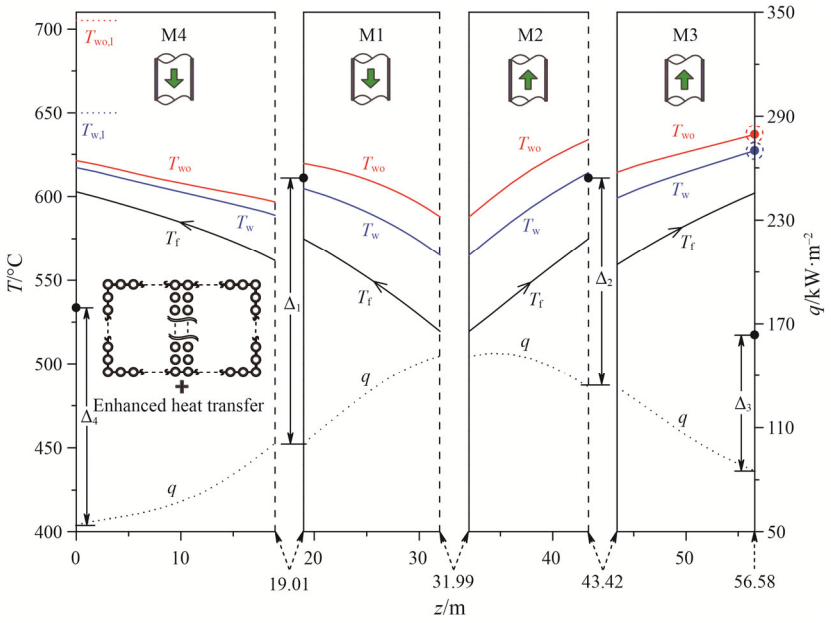

Fig. 15 Temperatures of modules with mid-partition wall, enhanced heat transfer and M1 and M4 flowing downwards under the optimal arrangement (4123)($\alpha_{f,e}$=1.5α_f, $T_{wo,max}$=636.74°C, $T_{w,max}$=627.23°C)

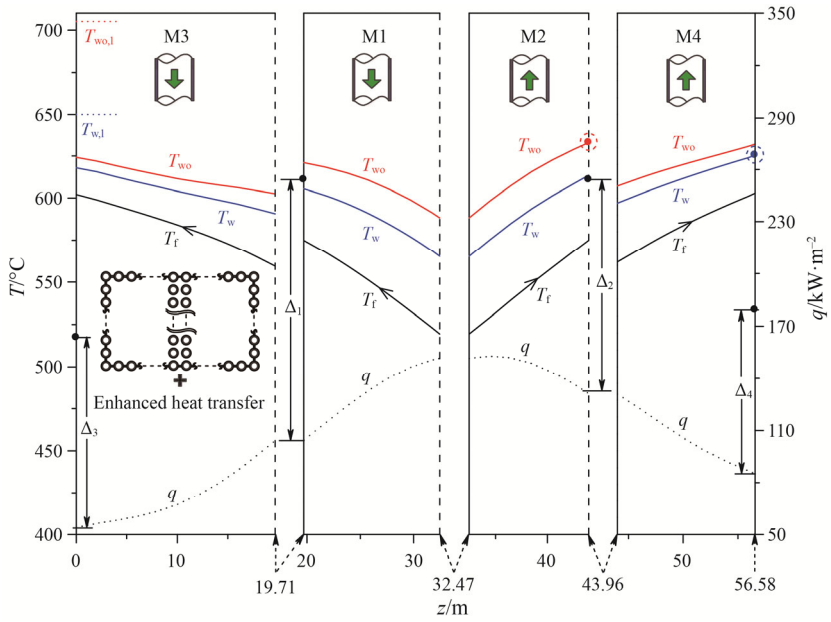

Fig. 16 Temperatures of modules with mid-partition wall, enhanced heat transfer and M1 and M3 flowing downwards under the new optimal arrangement (3124) ($\alpha_{f,e}$=1.5α_f, $T_{wo,max}$=632.83°C, $T_{w,max}$=625.43°C)

Table 4 Summary of $T_{w,max}$ and $T_{wo,max}$ under different module arrangements and measures

Case	Arrangement	Mid-partition wall/ Enhanced heat transfer/ Downward flow	$T_{w,max}$/°C /Position	$T_{wo,max}$/°C /Position
Case 1	1342 (worst)	N/N/N	678.45/M3	702.86/M3
Case 2	4123 (best)	N/N/N	649.31/M4	679.26/M1
Case 3	4123	Y/N/N	638.40/M4	651.12/M1
Case 4	4123	Y/Y/N	629.63/M4	641.61/M1
Case 5	4123	Y/Y/M4, M1	627.23/M3	636.74/M3
Case 6	3124 (new best)	Y/Y/M3, M1	625.43/M2	632.83/M4

The optimal arrangement of 3124 has $T_{w,max}$ of 625.43°C, 24.57°C lower than $T_{w,l}$, and $T_{wo,max}$ of 632.83°C, 72.17°C lower than $T_{wo,l}$. The average wall temperature of Module 3 and Module 1 is reduced to below 610°C, and thus the tube material can be degraded to decrease the cost.

6. Conclusions

The present work aims to build a proper matching strategy coupling the heat flux at the furnace side and tube side to reach the lowest hot spot temperature of cooling wall tubes in a sCO_2 boiler, which consists of four modules, each having different heat flux received from furnace side (q) and different CO_2 temperature in cooling wall tube (T_f). The comparison between the HTM and HHM methods are studied. The main conclusions are obtained as follows:

(1) The conventional HTM method could fail to obtain the optimal arrangement for sCO_2 modular cooling wall because the wall temperature depends not only on the temperature of sCO_2 and heat flux but also on the comprehensive thermal resistance. Moreover, the comprehensive thermal resistance varies among the modules in the cooling wall due to the different state parameters of sCO_2 within the tubes.

(2) The "allowable heat flux" integrates the sCO_2 temperature and the comprehensive thermal resistance, representing the maximum heat flux the tube can bear. The proposed HHM method of matching the allowable heat flux with local heat flux is a novel and comprehensive approach to control the cooling wall temperatures for sCO_2 boilers. For the sCO_2 boiler driving a 1000 MWe power plant, the cooling wall temperatures using HHM are smaller than those using HTM.

(3) The measures including mid-partition wall, heat transfer enhancement, and in-tube downward flow can effectively reduce the cooling wall temperature. The maximum mean wall temperature and outer wall temperature are decreased to 625.43°C and 632.83°C, which are 24.57°C and 72.17°C lower than the corresponding allowable wall temperatures, respectively.

Acknowledgment

The authors highly appreciate the support of the National Key R&D Program of China (2017YFB0601801), and the National Natural Science Foundation of China (No. 51776064).

References

[1] Dostal V., Hejzlar P., Driscoll M.J., The supercritical carbon dioxide power cycle: comparison to other advanced power cycles. Nuclear Technology, 2006, 154(3): 283–301.

[2] Dostal V., A supercritical carbon dioxide cycle for next generation nuclear reactors. Massachusetts Institute of Technology, Massachusetts, USA, 2004.

[3] Turchi C.S., Ma Z., Neises T.W., Wagner M.J., Thermodynamic study of advanced supercritical carbondioxide power cycles for concentrating solar power systems. Journal of Solar Energy Engineering, 2013, 135(4): 041007.

[4] Duniam S., Jahn I., Hooman K., Lu Y., Veeraragavan A., Comparison of direct and indirect natural draft dry cooling tower cooling of the sCO_2 Brayton cycle for concentrated solar power plants. Applied Thermal Engineering, 2018, 130: 1070–1080.

[5] Li M.J., Zhu H.H., Guo J.Q., Wang K., Tao W.Q., The development technology and applications of supercritical CO_2 power cycle in nuclear energy, solar energy and other energy industries. Applied Thermal Engineering, 2017, 126: 255–275.

[6] Al-Sulaiman F.A., Atif M., Performance comparison of different supercritical carbon dioxide Brayton cycles integrated with a solar power tower. Energy, 2015, 82: 61–71.

[7] Allam R.J., Fetvedt J.E., Forrest B.A., Freed D.A., The oxy-fuel, supercritical CO_2 Allam cycle: New cycle developments to produce even lower-cost electricity from fossil fuels without atmospheric emissions. Proceedings of ASME Turbo Expo 2014: Urbomachinery Technical Conference and Exposition, Düsseldorf, Germany, 2014, DOI: 10.1115/GT2014-26952.

[8] Allam R., Martin S., Forrest B., Fetvedt J., Lu X., Freed D., et al., Demonstration of the Allam Cycle: An update on the development status of a high efficiency supercritical carbon dioxide power process employing full carbon capture. Energy Procedia, 2017, 114: 5948–5966.

[9] Moullec L.Y., Conceptual study of a high efficiency coal-fired power plant with CO_2 capture using a supercritical CO_2 Brayton cycle. Energy, 2013, 49(1): 32–46.

[10] Mecheri M., Moullec L.Y., Supercritical CO_2 Brayton cycles for coal-fired power plants. Energy, 2016, 103: 758–771.

[11] Xu J., Sun E., Li M., Liu H., Zhu B., Key issues and solution strategies for supercritical carbon dioxide coal fired power plant. Energy, 2018, 157: 227–246.

[12] Yang Y., Bai W., Wang Y., Zhang Y., Li H., Yao M., et al., Coupled simulation of the combustion and fluid heating of a 300 MW supercritical CO_2 boiler. Applied Thermal Engineering, 2017, 113: 259–267.

[13] Yang D.L., Tang G.H., Fan Y.H., Li X.L., Wang S.Q., Arrangement and three-dimensional analysis of cooling wall in 1000 MW sCO_2 coal-fired boiler. Energy, 2020,

197: 117168.

[14] Park S., Kim J., Yoon M., Rhim D., Yeom C., Thermodynamic and economic investigation of coal-fired power plant combined with various supercritical CO_2 Brayton power cycle. Applied Thermal Engineering, 2018, 130: 611–623.

[15] Brun K., Friedman P., Dennis R., Fundamentals and applications of supercritical carbon dioxide (sCO_2) based power cycles. Woodhead Publishing, Oxford, 2017.

[16] Sun E., Xu J., Li M., Liu G., Zhu B., Connected-top-bottom-cycle to cascade utilize flue gas heat for supercritical carbon dioxide coal fired power plant. Energy Conversion Management, 2018, 172: 138–154.

[17] Sun E., Xu J., Hu H., Li M., Miao Z., Yang Y., Liu J., Overlap energy utilization reaches maximum efficiency for sCO_2 coal fired power plant: A new principle. Energy Conversion Management, 2019, 195: 99–113.

[18] Fan Q.G., Ultra-supercritical and subcritical boiler, China Electric Power Press, Beijing, 2007. (in Chinese)

[19] Wang S., Yang D., Liu D., Ouyang S., Wang W., Experimental and theoretical analysis on the safety and efficiency of an ultra-supercritical pulverized coal-fired boiler with low mass flux vertical water wall. Applied Thermal Engineering, 2019, 146: 440–449.

[20] Zhou J., Xiang J., Su S., Hu S., Wang Y., Xu K., et al., Key issues and practical design for cooling wall of supercritical carbon dioxide coal-fired boiler. Energy, 2019, 186: 115834.

[21] Che D., Zhuang Z., Li J., Wang D., Boiler, Xi'an Jiaotong University Press, Xi'an, 2008. (in Chinese)

[22] Hydraulic calculation method of utility boiler. Shanghai Power Equipment Packaged Design Research Institute, Beijing: Mechanical Industry Press, China, 1983. (in Chinese)

[23] Zhu X., Wang W., Xu W., A study of the hydrodynamic characteristics of a vertical water wall in a 2953t/h ultra-supercritical pressure boiler. International Journal of Heat and Mass Transfer, 2015, 86: 404–414.

[24] Zima W., Nowak-Ocłoń M., A new one/two-dimensional model of the conjugate heat transfer in waterwall tubes of the supercritical steam boiler combustion chamber. Heat Transfer Engineering, 2017, pp. 1–11.

[25] Tao W.Q., Numerical heat transfer, 2nd ed., Xi'an Jiaotong University Press, Xi'an, 2001. (in Chinese)

[26] Chen D., Fan C., Yang Y., Zhang F., Zhu C., Study on water wall temperature and heat load distribution in 1000 MW tower-type once-through boilers. Journal of Chinese Society of Power Engineering, 2013, 33(5): 329–334. (in Chinese)

[27] Brown, Glenn O., The history of the Darcy-Weisbach equation for pipeflow resistance. American Society of Civil Engineers, 2002, pp. 34–43.

[28] Liu Z.B., He Y.L., Yang Y.F., Fei J.Y., Experimental study on heat transfer and pressure drop of supercritical CO_2 cooled in a large tube. Applied Thermal Engineering, 2014, 70(1): 307–315.

[29] Sheng C., Chen T., Derivation for radiation angle factor of membrane waterwall with rectangular fins. Boiler Technology, 1997, 08: 8–11. (in Chinese)

[30] Zhang Q., Li H., Lei X., Zhang J., Kong X., Study on identification method of heat transfer deterioration of supercritical fluids in vertically heated tubes. International Journal of Heat and Mass Transfer, 2018, 127: 674–686.

[31] Mokry S., Pioro I., Kirillov P., Gospodinov Y., Supercritical-water heat transfer in a vertical bare tube. Nuclear Engineering and Design, American Society of Mechanical Engineers, 2010, 240: 568–576.

[32] Wu G., Bi Q., Yang Z., Wang H., Zhu X., Hao H., et al., Experimental investigation of heat transfer for supercritical pressure water flowing in vertical annular channels. Nuclear Engineering and Design, 2011, 241(9): 4045–4054.

[33] Lemmon E.W., Huber M.L., Mc Linden M.O., NIST standard reference database 23: reference fluid thermodynamic and transport properties-REFPROP, version 9.1. Tech. rep. Gaithersburg: National Institute of Standards and Technology, Standard Reference Data Program, 2013.

[34] Selectiong guide for the metallic material of fossil power plants. Power industry standards of People's Republic of China, Beijing, China, 2015. (in Chinese)

[35] Water-tube boilers-Part 4: Strength calculation of pressure parts. National standards of People's Republic of China, Beijing, China, 2013. (in Chinese)

[36] Zima W., Nowak-Ocłoń M., Ocłoń P., Novel online simulation-ready models of conjugate heat transfer in combustion chamber waterwall tubes of supercritical power boilers. Energy, 2018, 148: 809–823.

[37] Pan J., Yang D., Chen G., Zhou X., Bi Q., Thermal-hydraulic analysis of a 600 MW supercritical CFB boiler with low mass flux. Applied Thermal Engineering, 2012, 32: 41–48.

[38] Huang D., Wu Z., Sunden B., Li W., A brief review on convection heat transfer of fluids at supercritical pressures in tubes and the recent progress. Applied Energy, 2016, 162: 494–505.

[39] Wang Y., He Y.L., Lei Y.G., Zhang J., Heat transfer and hydrodynamics analysis of a novel dimpled tube. Experimental Thermal and Fluid Science, 2010, 34(8): 1273–1281.